

Low-temperature glasslike properties in $(\text{NaCl})_{1-x}(\text{NaCN})_x$

Susan K. Watson* and R. O. Pohl

Cornell University, Ithaca, New York 14853

(Received 6 September 1994)

Thermal conductivity, internal friction, transverse sound velocity (60 mK to 300 K), and specific-heat data (100 mK to 40 K) for $(\text{NaCl})_{1-x}(\text{NaCN})_x$ ($x=0, 0.025, 0.05, 0.1, 0.76, 1$) show a progression from crystalline to glasslike behavior as the CN^- concentration is increased from 0 to 76%. The evolution of glasslike properties is compared to that in other crystals in which glasslike properties evolve with increasing disorder, e.g., $(\text{KBr})_{1-x}(\text{KCN})_x$ and $\text{Ba}_{1-x}\text{La}_x\text{F}_{2-x}$. For $(\text{KBr})_{1-x}(\text{KCN})_x$, Sethna and Chow have shown that as the concentration of the almost freely rotating CN^- ions is increased the average potential barrier for CN^- reorientation also increases through elastic quadrupolar interactions. For $x \sim 0.5$, only a small density of low-energy states is left, which equals that observed in structural glasses. In $\text{Ba}_{1-x}\text{La}_x\text{F}_{2-x}$, on the other hand, the crystal field for small doping x is so large that no atomic motion occurs at low temperatures. $(\text{NaCl})_{1-x}(\text{NaCN})_x$ is shown to represent an intermediate case, in that the crystal field is non-negligible at small x , yet glasslike low-energy excitations indicative of very small potential barrier heights evolve with increasing x . It is argued that random internal strains cause a decrease of the barrier heights in these crystals, which lead to the low-energy excitations. It is proposed that random strains have a similar effect in other disordered crystals as in $\text{Ba}_{1-x}\text{La}_x\text{F}_{2-x}$, which for small x show no low-energy mobile states, yet which for large x become glasslike.

I. INTRODUCTION

For nearly 20 years the phenomenological tunneling model^{1,2} has provided a powerful conceptual framework for analyzing the properties of amorphous solids. Despite its successes, however, many fundamental questions remain regarding the low-energy excitations (referred to as two-level systems, TLS) in glasses. Amorphous solids are not the only solids with low-temperature thermal and elastic properties that are dominated by TLS. Certain mixed crystalline solids with substitutional disorder, such as the mixed alkali-halide cyanides, show the same effects.³ The systems retain their crystalline order, making them simpler to model than amorphous solids, and their degree of disorder can be easily changed by varying the concentration of constituents. Consequently, mixed crystals with glasslike properties have proven to be very useful for studying both the TLS and phase transitions in glasses.

The system studied in this paper, $(\text{NaCl})_{1-x}(\text{NaCN})_x$, belongs to a class of materials where the elongated CN molecule is randomly substituted for a halide atom in an alkali-halide host, $(\text{MX})_{1-x}(\text{M}(\text{CN}))_x$ where M refers to an alkali metal and X refers to a halogen ion. The reader is referred to the literature for a review of their properties.⁴⁻⁷ For the present work we note that for intermediate CN^- concentrations the CN^- ordering and structural phase transitions which occur in the pure alkali cyanides are suppressed due to a competition between lattice-mediated interactions between CN^- which favor ordering and random strain fields which act against it.⁵⁻⁷ The low-temperature thermal and elastic properties in

this same concentration range are dominated by TLS.

We will explore the roles of disorder and elastic quadrupolar interactions in producing the broad energy distributions found in the mixed alkali-halide cyanides by comparing the thermal and elastic properties of $(\text{NaCl})_{1-x}(\text{NaCN})_x$ and $(\text{KBr})_{1-x}(\text{KCN})_x$. In $(\text{KBr})_{1-x}(\text{KCN})_x$ the TLS are believed to evolve from individual CN^- which reorient by 180° via quantum-mechanical tunneling at low temperature and small CN^- concentrations. Sethna and Chow⁸ have persuasively argued that as the CN^- concentration is increased, elastic quadrupolar interactions between the CN^- cause the potential barriers for reorientation to increase for the majority of CN^- , leaving a small fraction with the appropriate tunnel splitting energy to give the universal glasslike properties.

For $(\text{NaCl})_{1-x}(\text{NaCN})_x$, on the other hand, the average potential barrier for reorientation (i.e., the crystal field) is already large at low CN^- concentrations. In effect, the CN^- orientations are frozen in at low temperatures. Increasing the CN^- concentration should further increase the potential barriers for reorientation for the majority of CN^- , assuming that quadrupolar interactions between CN^- dominate and that the crystal field can be ignored, as in the Sethna-Chow model. This leads to an interesting question: Is it possible for $(\text{NaCl})_{1-x}(\text{NaCN})_x$ to show glasslike thermal and elastic properties which, after all, require the presence of TLS with relatively low potential barriers? This question is closely related to that of the occurrence of glasslike excitations in many highly disordered crystals.⁹ In $\text{Ba}_{1-x}\text{La}_x\text{F}_{2-x}$, for example,¹⁰ low-energy excitations have not been found for $x \leq 0.01$, yet evolve gradually for larger x , approaching the proper-

ties of amorphous solids for $x \geq 0.1$. What role, if any, do the crystal field, elastic dipoles and their interaction play in this or similar cases?

The paper begins with a comparison of the known properties of $(\text{NaCl})_{1-x}(\text{NaCN})_x$ with those of $(\text{KBr})_{1-x}(\text{KCN})_x$ which will help put the present work in context. This is followed by a description of the sample preparation and experimental methods. Our data are then presented and discussed.

II. BACKGROUND

Before it was recognized that the mixed alkali-halide cyanides exhibit glasslike properties at intermediate CN^- concentrations ($x \sim 0.5$), alkali halides doped with small concentrations of cyanide ($x \leq 0.001$) were used to study the ways in which tunneling centers are influenced by the crystal field in which they are embedded.^{11,12} This early work showed that the potential barrier that an isolated CN^- experiences varies considerably between alkali-halide hosts.

Several experimental techniques demonstrated that the potential barrier for reorientation of an isolated CN^- ion is larger in NaCl than in KBr. From IR absorption measurements, Seward and Narayanamurti¹¹ deduced a potential barrier more than three times larger in NaCl ($V \geq 0.01$ eV for 0.1% CN^-) than in KBr ($V \sim 0.003$ eV for 0.3% CN^-). From ultrasonic velocity and attenuation experiments, Byer and Sack determined that the barriers for the CN^- in NaCl are ~ 0.035 eV for the 0.1% CN^- .¹³ Thermal conductivity measurements on 0.05% CN^- in KBr were found to be consistent with the IR results. The lower potential barrier in KBr results in a larger tunnel splitting of the ground state of the CN^- ion, leading to strong resonant scattering in the thermal conductivity at a temperature (~ 500 mK) consistent with the energy-level spacing of the CN^- in the lattice.¹¹ For 0.27% CN^- in NaCl, by contrast, no resonant scattering was evident in the thermal conductivity below 1 K, from which Seward and Narayanamurti deduced that the potential barrier was larger than 0.017 eV.¹¹ The large potential barrier in NaCl results in a small enough ground-state splitting that resonant scattering might appear at lower temperatures, outside of the experimental window. In addition, since the scattering rate is proportional to the energy-level spacing, the smaller ground-state splitting results in less phonon scattering.¹⁴ The CN^- orientations in NaCl are essentially frozen in at low concentrations and temperatures.

Figure 1 dramatically illustrates the different effect on the thermal transport of small concentrations of CN^- in the two alkali-halide hosts. Phonons in KBr+0.3% CN^- are strongly scattered by the tunneling states of the CN^- , leading to a thermal conductivity (solid circles) that is orders of magnitude smaller than for pure KBr. The same concentration of CN^- in NaCl (solid triangles), however, has nearly no effect on the thermal conductivity below 1 K where resonant scattering from tunneling centers should show up. The presence of CN^- only be-

comes apparent at higher temperatures where other sources of phonon scattering dominate. Near 10 K, the random substitution of CN^- for Cl^- results in point defect scattering of the phonons, reducing the thermal conductivity of NaCl+0.3% CN^- below that of NaCl. There is a slight dip in the data near 40 K, similar to a depression in the thermal conductivity data of $\text{KBr}_{0.05}\text{KCl}_{0.95}$ which has been ascribed to a resonant mode from the Br^- in KCl.¹⁵ Seward and Narayanamurti speculated that the dip in their data for NaCl+0.3% CN^- may have been caused from either a resonant mode of the CN^- in NaCl or from resonant scattering of phonons from the higher CN^- energy levels near the top of the reorientational potential barrier.¹¹

The size of the potential barrier for reorientation of CN^- is not the only difference between the two host lattices. Low-temperature heat-capacity measurements, which probe the energy spectrum of both the phonons and the CN^- tunneling centers, reveal that the tunneling levels of the CN^- in NaCl are more strongly influenced by changes in their local environments than CN^- in KBr. For small concentrations of CN^- in KBr, the CN^- tunneling centers are isolated and have nearly identical environments, resulting in a similar energy spectrum for each CN^- . Under such circumstances a Schottky peak

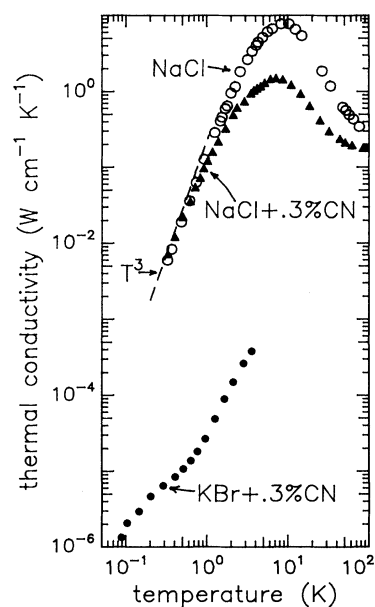


FIG. 1. Comparison of the thermal conductivity of $(\text{NaCl})_{1-x}(\text{NaCN})_x$ ($x=0$ and 0.003, Ref. 11) and $(\text{KBr})_{0.997}(\text{KCN})_{0.003}$ (Ref. 4) for low CN^- concentrations. The curve marked T^3 indicates the Casimir limit for the $(\text{NaCl})_{1-x}(\text{NaCN})_x$ samples (cross sections: 0.5×0.5 cm², Ref. 11). Below 1 K, resonant scattering from the CN^- tunneling levels dominates the thermal conductivity of KBr+0.3% CN. The same concentration of CN^- in NaCl, however, produces no significant resonant scattering below 1 K, indicating a combination of larger reorientational barriers, and perhaps, weaker coupling.

in the heat capacity is expected in addition to the T^3 lattice contribution (or a broadened peak if a few closely spaced energy levels are involved; see, for example, Ref. 11). If the CN^- remain independent, the peak should simply scale with the CN^- concentration, which is approximately the case for concentrations less than $\sim 0.3\%$ CN^- in KBr (Refs. 16 and 17) [Fig. 2(a); see also Fig. 7 of Ref. 4]. The low-temperature tails in the solid curves of Fig. 2(a) (Refs. 4 and 16) are believed to be due to residual strain in the crystals.¹⁸ The dash-dotted line is a

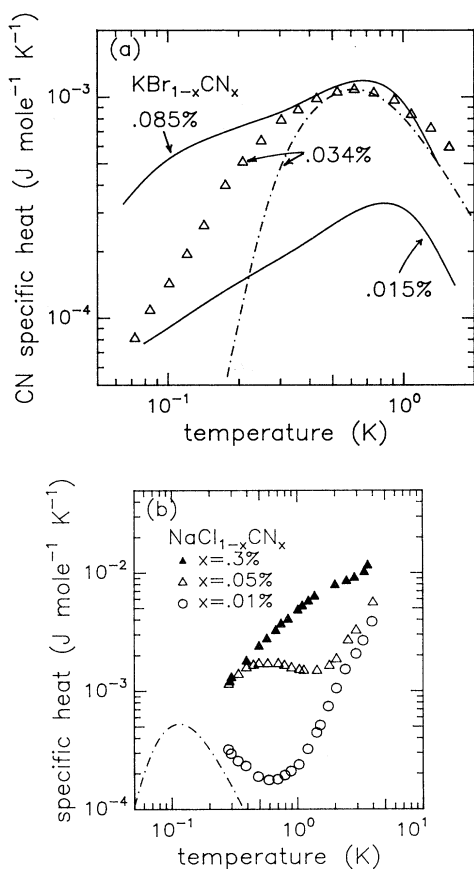


FIG. 2. (a) Specific-heat contribution of CN^- tunneling centers to KBr (i.e., heat capacity with lattice contribution subtracted) after Ref. 17. The peak in the Schottky type anomaly remains at the same temperature and approximately scales with the CN^- concentration. Solid lines are from Ref. 16; see also Ref. 4. The low-temperature tails in the data are believed to be due to residual strain in the crystals. Data for 0.034% CN^- (open triangles) and Schottky peak calculated for 0.034% $\langle 111 \rangle$ -oriented CN^- in KBr (dash-dotted line) are from Ref. 17 (see text). (b) Total (lattice and CN^- tunneling center) specific heat of $(\text{NaCl})_{1-x}(\text{NaCN})_x$ for low CN^- concentrations, Ref. 19. A specific-heat anomaly appears to shift to higher temperature with increasing concentration. The dash-dotted line is an estimate of the Schottky-type anomaly expected for $x=0.01\%$ in $(\text{NaCl})_{1-x}(\text{NaCN})_x$ based upon the estimated energy levels of 0 cm^{-1} (degeneracy $\equiv g_0=1$), 0.21 cm^{-1} ($g_1=2$), and 0.36 cm^{-1} ($g_2=3$); see text.

Schottky-type peak for 0.34% CN^- in KBr calculated by Dobbs, Foote, and Anderson for a $\langle 111 \rangle$ -oriented CN^- molecule in KBr with four energy levels of degeneracy 1-3-3-1 separated by 1.0 cm^{-1} .¹⁷ The $(\text{NaCl})_{1-x}(\text{NaCN})_x$ data of Seward, Reddy, and Shaner,¹⁹ however, are quite different over a similar CN^- concentration range [see Fig. 2(b)]. For 0.01% CN^- in NaCl (open circles) there is a sharp upturn in the heat-capacity data below 0.5 K, suggesting the presence of a Schottky-type anomaly below the experimental temperature window. Upon increasing the CN^- concentration from $x=0.01$ to 0.05% (open triangles), a peak is visible, and at $x=0.3\%$ (solid triangles) it moves to higher temperatures and broadens considerably. The dash-dotted line in Fig. 2(b) is a Schottky-type peak calculated for 0.01% CN^- in NaCl assuming six energy levels [ground state, first excited state ($\Delta_1=0.21 \text{ cm}^{-1}$) with a degeneracy of two, and a second excited state ($\Delta_2=0.36 \text{ cm}^{-1}$) with a degeneracy of three] appropriate for the $\langle 100 \rangle$ orientations of the CN^- in NaCl.⁷ For the tunnel splittings of the CN^- in NaCl, we assume that the splittings scale with the potential barriers as $V^{1/2} \exp(-a_0 V^{1/2})$ (where a_0 is a constant assumed to be the same for CN^- in KBr and NaCl) so that for NaCl, where the barriers are roughly nine times larger than in KBr or KCl, the tunnel splittings for the CN^- are seven times smaller than in KCl.¹¹ [The tunneling state energies for $\langle 100 \rangle$ -oriented CN^- in KBr and KCl are 1.4 cm^{-1} (for the T_{1u} state) and 2.4 cm^{-1} (for the E_g state).^{11,12}]

From the observed shift and broadening of the Schottky-type peak in $(\text{NaCl})_{1-x}(\text{NaCN})_x$, Seward, Reddy, and Shaner¹⁹ concluded that the tunnel splitting of the ground state is determined largely by interactions between cyanides. However, lattice-mediated interactions between cyanides are not the only effect of introducing more CN^- into NaCl. Due to the size disparity of the lattice constants of NaCl and NaCN (Table I) random strains are also introduced. Since it is possible, in theory, for random strains to broaden the asymmetry distribution of the tunneling centers,²³ some of the broadening of the peaks in $(\text{NaCl})_{1-x}(\text{NaCN})_x$ data may originate from these static internal strains. Theoretical studies by Michel of the mixed alkali-halide cyanides at higher CN^- concentrations have underscored the importance of the static random strain fields on the structural phase transitions.⁵ The author has argued that dynamic and

TABLE I. Room-temperature lattice constants a and number densities N for alkali halides and alkali cyanides referred to in this work. For the rocksalt structure the number density of each constituent is $N=4/a^3$.

Material	a (\AA)	N (cm^{-3})	Reference
NaCl	5.64	2.23×10^{22}	20
NaCN	5.85	2.00×10^{22}	This work
KBr	6.593	1.396×10^{22}	21
KCl	6.293	1.605×10^{22}	20
KCN	6.523	1.441×10^{22}	22

static strain have an impact on both the elastic quadrupoles (T_{2g} or E_{1u} symmetry, also referred to as "elastic dipoles") and the small electric dipole moment (T_{1u} symmetry) which should have the relevant symmetry for the low-temperature TLS. NMR experiments probing the Na^+ ions at the glass transition in $(\text{NaCl})_{0.35}(\text{NaCN})_{0.65}$ support the view that random strains are significant.²⁴

Structural studies have shown that both $(\text{KBr})_{1-x}(\text{KCN})_x$ and $(\text{NaCl})_{1-x}(\text{NaCN})_x$ have high-temperature cubic phases on the CN^- -rich side of the phase diagram, stabilized by the rapid reorientation of the CN^- , and low-temperature glasslike ($x \leq x_c$) or ordered phases ($x \geq x_c$), where x_c is the critical concentration below which phase transitions into ordered phases are suppressed. Due to the differences between the ionic radii and lattice constants of the systems, the critical concentrations are material dependent: $x_c \sim 0.8$ for $(\text{NaCl})_{1-x}(\text{NaCN})_x$ and $x_c \sim 0.6$ for $(\text{KBr})_{1-x}(\text{KCN})_x$.⁶ In other words, the phase transitions which result from the lattice-mediated interactions between the CN^- are more easily suppressed by dilution of the CN^- in $(\text{NaCl})_{1-x}(\text{NaCN})_x$, the system with the larger random internal strain field, than in $(\text{KBr})_{1-x}(\text{KCN})_x$.

III. EXPERIMENTAL MATTERS

A. Thermal conductivity

The thermal conductivity below 30 K was measured using the steady-state temperature gradient method with two thermometers [100- Ω Allen Bradley resistors with two 20-cm, 0.076-mm diameter constantan (advance) wire leads above 1.5 K; 200- Ω Matsushita resistors with two 4-cm, 0.05-mm diameter Pt:W wire leads below 1.5 K] and one metal film heater (1000 Ω with two 20-cm, 0.076-mm diameter constantan wire leads above 1.5 K and with two 1-cm, 0.05-mm diameter Pt:W wire leads below 1.5 K). Thermometers and heaters were epoxied to Cu foil with Stycast 2850. The foil was soldered to bare Cu wire (~ 0.3 mm diameter) which was wrapped twice around the sample and glued with GE 7031 varnish. The thermometers were calibrated during each run (with no heat into the sample) against Ge thermometer standards mounted on the stages of a dilution refrigerator and a "dipper cryostat" which can be inserted into a ^4He storage dewar, as described in Ref. 25. The dipper cryostat provided insufficient cooling power to allow measurement of the large thermal conductivity of NaCl above 1.5 K. Instead, we used a conventional ^4He cryostat for this sample. Due to the uncertainty associated with determining the cross-sectional area of the sample and the separation between thermometers, the thermal conductivity data are accurate to within $\pm 15\%$. The precision, however, is on the order of a few percent.

Data above 30 K were taken by an ac technique, the "3 ω method," for which the effects of blackbody radiation, which plague dc measurements above ~ 80 K, are negligible.²⁶ This method is also well suited for measurements of thin samples. For the present study, samples ($8 \times 8 \times 3$ mm³) were attached (with Dow-Corning 200

fluid) to the stage of a ^4He dipper cryostat. Thermal equilibration times were very short.

B. Heat capacity

Heat capacities were measured with the transient heat-pulse technique. The precision of the data is on the order of a few percent. From the outset we should warn that there is some uncertainty in the magnitude of the heat-capacity data below 1 K for $x=0.05$ and 0.1. The internal equilibrium times for these mixed crystals were long enough to be noticeable on a time scale of several minutes. As a result, the temperature variation of the samples was nonexponential after application of the heat pulse, making determinations of the total temperature change ΔT , and hence, $C=(\Delta Q)/(\Delta T)$ uncertain (C =heat capacity; ΔQ =heat input) (see Fig. 3). Similar

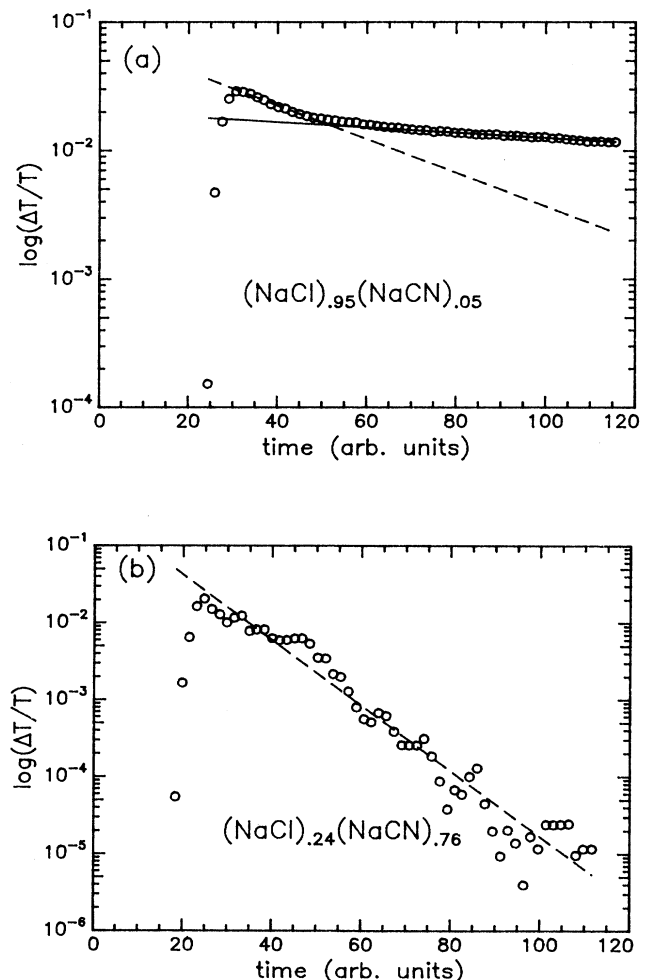


FIG. 3. Temperature decays (with baseline temperature subtracted) after application of heat pulse for (a) $x=0.05$, and (b) $x=0.76$ at $T=200$ mK. For $x=0.05$ there is evidence of both short (dashed line) and long (solid line) relaxation times. For $x=0.76$ there are only short relaxation times (dashed line); the large scatter at the tail occurs as the temperature decay approaches the baseline.

behavior had been seen for $(\text{NaCl})_{1-x}(\text{NaCN})_x$ by Seward, Reddy, and Shaner who concluded from the long internal equilibration times that the CN^- in NaCl are more weakly coupled to the lattice than in KBr.¹⁹ The net result is that the data for $x=0.05$ and $x\sim 0.10$ are most likely an *underestimate* of the actual specific heat. (If only a fraction of the states have been excited on the time scale of the heat release, the tunneling defects will not be in equilibrium with the lattice and the change in the lattice temperature after the heat pulse ΔT will be artificially large.) Two data runs using different thermometers were performed for the sample with $x=0.05$ in order to check whether the nonexponential temperature decays were an experimental artifact. The two runs resulted in nearly identical specific-heat data (to within $\pm 5\%$), supporting our belief that the effects are intrinsic; only one data set is shown in the figures for clarity. Note that for pure NaCl and NaCN, and for $x=0.76$, the internal equilibration times were small enough that the temperature decays were exponential [e.g., Fig. 3(b)].

For measurements below 1 K, samples of ~ 3 g were clamped between sapphire pins to the stage of a dilution refrigerator. The small contact area between the sample and pins combined with the large Debye temperature of sapphire ensures that the sample mount makes a relatively minor contribution to the heat capacity. The thermometer (a ground down, 10 mg, 100- Ω Matsushita resistor with two 3-cm, 0.05-mm diameter Nb:Ti wire leads) and the heater (a 500- Ω metal film resistor deposited on sapphire with two 2-cm, 0.05-mm diameter Nb:Ti wire leads) were glued to cleaved faces of the samples using GE 7031 varnish. Sample-to-bath thermal time constants were on the order of 20 min at 100 mK decreasing to ~ 2 min at 1.5 K for $x=0.05$ and ~ 15 sec over the entire temperature range for the NaCl and NaCN samples. The doped samples, $x\sim 0.1$ and $x=0.76$, had time constants between these two extremes.

The heat capacity due to the addenda was determined by measuring the specific heat of a high purity KBr crystal and assigning the addenda to the heat capacity in excess of the T^3 lattice contribution taken from the literature.⁴ The addenda heat capacity was subtracted from all data sets except for the NaCl sample, where a different thermometer was used and no addenda data are available. The thermometer used for the NaCl data was nearly identical in construction to two other thermometers for which the addenda heat capacities were measured and were found to agree to within $\pm 20\%$. In Sec. IV B we use the addenda of these other thermometers as an estimate of the addenda for NaCl. For the NaCN sample the addenda heat capacity was comparable to that of the sample at the lowest temperature and dropped to less than 10% by 500 mK. For the mixed crystals, the addenda made a contribution of less than 10% over the entire temperature range.

Above 1.5 K the heat capacity was measured in a dipper cryostat. Application of the technique to the alkali-halide cyanides is described in more detail in Ref. 27. Typical sample masses were 300 mg. The thermal link to the calorimeter was through two heater leads (5-cm long, 0.127-mm diameter brass wire) giving sample-

to-bath thermal time constants on the order of 10 sec at 1.5 K and increasing to roughly 1 h at 50 K. A ground down Allen Bradley resistor with two 3-cm, 0.05-mm diameter Pt:W leads served as a thermometer and was calibrated during each run against a Ge thermometer standard mounted on the copper stage of the dipper cryostat.

For measurements above 1.5 K, the heat capacity of the addenda, due to the calorimeter with no sample mounted and due to materials used for mounting the samples (1-mg Apiezon N grease, 1-mg GE 7031 varnish, 50-mg sapphire) was measured separately, as described in Ref. 27. The addenda contributed less than 10% over the entire temperature range and have been subtracted from the data.

C. Internal friction

The internal friction Q^{-1} was measured in torsion at an excitation frequency of ~ 90 kHz using a composite oscillator technique (with samples epoxied to a quartz transducer) which ensures good thermal contact between the sample and the cryostat.²⁸ Crystals were cleaved along $\{100\}$ faces, resulting in torsional motion around $\langle 100 \rangle$ directions. Samples epoxied directly to the quartz transducer with Stycast 2850 repeatedly cracked during cooldown because of differential thermal contraction, as evidenced by sudden shifts of the resonant frequency ($\sim 1\%$) of the composite quartz-sample structure. This cracking was avoided by epoxying a 0.25 mm layer of indium foil between the sample and transducer using Stycast 2850.

The internal friction due to the mounting arrangement was measured in a separate run by affixing a quartz sample (i.e., a material with low internal friction) to the transducer with 0.25 mm of indium foil sandwiched in-between (and epoxied with Stycast 2850). These data are referred to as the background and have not been subtracted from the data for the alkali-halide cyanides.²⁹ Although the precision of the measurements is typically a few percent, the accuracy is dominated by the uncertainty in the moments of inertia of the samples. Since the alkali-halide samples were sanded by hand to achieve the desired length and cross section, the uncertainty in the moment of inertia, and, hence Q^{-1} , is $\pm 20\%$ for $x=0.025, 0.05$, and ~ 0.1 . Due to the limited availability of material, the sample dimensions and moment of inertia for the $x=0.76$ sample were much smaller than for the other concentrations. As a result, we pushed the limits of applicability of the equations used to convert the measured loss of the composite transducer-sample structure to the loss of the sample alone. To take this into account, we conservatively add another $\sim 20\%$ uncertainty, resulting in a total uncertainty of $\pm 40\%$ for $x=0.76$.

Data from 300 to 1.4 K were taken in a dipper cryostat,²⁵ while slowly cooling the sample stage and monitoring the magnitude of the signal at the resonance frequency, f_0 (see Ref. 28). Below 1.4 K the sample stage of the dilution refrigerator was temperature controlled and the internal friction was determined directly from the full width at half maximum of the square of the amplitude of the resonance peak by performing a frequency scan from

$f_0 - 2\Delta f$ to $f_0 + 2\Delta f$, where Δf is the full width at half maximum. Self-heating of the sample was checked at the lowest temperature (~ 70 mK) by varying the input power by over two orders of magnitude and testing for any variation in the value of Q^{-1} . The input power was kept at a factor of 2 below the value ($\sim 3\%$ variation in Q^{-1}) where self-heating effects first became noticeable.

The internal friction of the composite structure (quartz transducer + sample) is the quantity directly measured. The internal friction of the sample is easily determined from the data for the composite oscillator and the moments of inertia of the sample and transducer, as outlined in Ref. 28 (see also Ref. 30). The transverse speed of sound is obtained simultaneously from the resonant frequency of the sample.³⁰

D. Sample preparation

NaCl crystals were seed pulled from the melt using chlorine-treated NaCl powder to minimize the OH^- content. The crystals were further purified by repeated seed pullings in which the bottom third of the crystal was discarded before the subsequent pull. After three seed pullings the typical OH^- content was 0.1 to 0.2 ppm, as revealed by uv analysis of the OH^- peak at 185 nm ($N = \sigma\alpha$, where N is the concentration of OH^- in ppm, α is the absorption coefficient in cm^{-1} , and σ is the absorption cross section; for OH^- in NaCl, $\sigma = 1.3 \text{ ppm/cm}^{-1} = 2.9 \times 10^{16} \text{ cm}^{-2}$, Ref. 31). From a comparison of the thermal conductivity of our NaCl crystal with data for NaCl intentionally doped with a range of OH^- concentrations determined by chemical analysis,³² a concentration of 0.5-ppm OH^- was estimated for our sample, close to the value from the uv analysis.

A NaCN crystal was seed pulled from the melt at Cornell, using NaCN powder from E. Merck Industries, Germany, as the starting material. Although precautions were taken to remove H_2O by carefully vacuum baking the NaCN powder from which the crystal was grown, without zone refinement the resulting NaCN crystal had a significant NCO^- concentration (2000 ppm as revealed by IR analysis of the NCO^- peaks³³). The NaCN crystal was used for growing the mixed crystal with the smallest concentration of CN^- , $\text{NaCl}_{0.975}\text{NaCN}_{0.025}$ (composition in solid), resulting in OH^- and NCO^- impurity concentrations of 3 and 130 ppm, respectively.

For the higher CN^- concentration samples ($x = 0.05$, composition in solid; $x = 0.20$, composition in melt), we used zone-refined NaCN crystals purchased from M. DeLong (crystal growing facility, University of Utah, Salt Lake City). The $\text{NaCl}_{0.24}\text{NaCN}_{0.76}$ (composition in solid) mixed crystal was provided by K. Knorr from Mainz, Germany and J. Albers from Saarbruecken University, Germany.

Cyanide concentrations in the $x = 0.025$ and 0.05 samples were determined from IR analysis of the CN^- stretch mode at 2104 cm^{-1} using a cross section of $\sigma = 1.8 \times 10^{19} \text{ cm}^{-2}$.¹¹ The IR absorption was so large for the $x = 0.20$ sample that we were unable to cleave a thin enough piece to determine the CN^- concentration. Based upon the fact that the concentrations in the solid

for the $x = 0.025$ and 0.05 samples were one-half the values in the melt, we estimate that the concentration in the solid is $x \sim 0.10$ for the sample with $x = 0.20$ in the melt. Throughout this work we refer to the sample as containing $\sim 10\% \text{CN}^-$.

We end this section with a word of advice and a word of caution regarding the growth of NaCl:CN mixed crystals. One feature of $(\text{KBr})_{1-x}(\text{KCN})_x$ which makes it attractive to study is the complete miscibility of the constituents over the full CN^- concentration range due to the similarity in lattice size of KBr and KCN (see Table I). For $(\text{NaCl})_{1-x}(\text{NaCN})_x$, on the other hand, the size disparity of NaCl and NaCN (Table I) makes these materials difficult to grow at intermediate concentrations. Krüger *et al.*³⁴ have found that for CN^- concentrations above 63%, it is useful to start with pure NaCN and introduce $\sim 10\%$ NaCl with each seed pulling. In other words, it is best to start with the material with the larger lattice constant, NaCN, and successively add more NaCl. Alternatively, one can attempt to grow the desired mixed crystal in one seed pulling using the proper concentrations of NaCl and NaCN. We have found that this approach becomes increasingly difficult above concentrations of $\sim 20\%$ due to the nucleation of small crystallites.

Krüger *et al.* have shown through Brillouin scattering and heat-capacity experiments on $(\text{NaCl})_{1-x}(\text{NaCN})_x$ ($0.63 \leq x \leq 1$) that there are significant concentration gradients along the draw axes of the $(\text{NaCl})_{1-x}(\text{NaCN})_x$ crystals ($\sim 0.3\%$ per mm) and even along an axis perpendicular to the draw axis ($\sim 0.7\%$ per mm).³⁴ Our data for the thermal conductivity, heat capacity and internal friction, therefore, represent those quantities for a spread of concentrations about an average value. For the present work, typical sample sizes are $1.5 \times 0.3 \times 0.3 \text{ cm}^3$ for thermal conductivity runs, $1.5 \times 0.7 \times 0.7 \text{ cm}^3$ for heat-capacity runs in the dilution refrigerator, $0.3 \times 0.8 \times 0.8 \text{ cm}^3$ for heat capacity runs in the dipper cryostat, and $1 \times 0.4 \times 0.4 \text{ cm}^3$ for internal friction runs.

IV. EXPERIMENTAL RESULTS

A. Thermal conductivity

The thermal conductivity of $(\text{NaCl})_{1-x}(\text{NaCN})_x$ (Fig. 4) shows a clear progression from crystalline to glasslike behavior as the CN^- concentration is increased. The data for pure NaCl (solid line, Ref. 11, and plusses, this work) and for $x = 0.003$ (dashed line, Ref. 11 and open diamonds, this work) are crystalline in form. In particular, they exhibit a peak near 10 K and approach a T^3 temperature dependence (Casimir boundary scattering regime) below 1 K. Our two data points for pure NaCl (plusses) are slightly lower than the data from Ref. 11, indicating the somewhat larger OH^- content in our crystal (0.1–0.5 ppm for ours compared to ~ 0.1 ppm for theirs.¹¹)

The thermal conductivity data for $x = 0.025$ (open circles) also approach T^3 behavior below 300 mK, indicating that the material is still in the crystalline concentration range of the phase diagram. The dash-dotted line marked " T^3 " indicates the Casimir limit calculated from

TABLE II. Material parameters used for analyzing the $(\text{NaCl})_{1-x}(\text{NaCN})_x$ data. The room-temperature mass density ρ of NaCl was measured by the flotation method, while those of $x \sim 0.1$, $x = 0.76$ and pure NaCN were determined both from room-temperature x-ray analyses of our samples and from the flotation method, with agreement between techniques to within 2%. The Debye temperature (Θ_D) and velocity (v_D) for NaCl are from Ref. 38 using the lattice constant from Table I to convert between Θ_D and v_D . The Debye temperature and velocity for NaCN are determined from a T^3 fit to our heat-capacity data using a room-temperature lattice constant of 5.85 Å from our x-ray measurements to convert between Θ_D and v_D . The Debye velocities for $x = 0.025$ and 0.05 were estimated from the values for NaCl and NaCN and the relation $\Theta_D^{-2} = x\Theta_{D1}^{-2} + (1-x)\Theta_{D2}^{-2}$ (Ref. 39); the expression is appropriate for alloys and does not take into account the softening for the alkali halide-cyanide mixed crystals. Transverse speeds of sound for NaCl and NaCN were estimated from the expressions $v_D^{-1} = 3^{-1/3} \times (v_l^{-3} + 2v_t^{-3})^{1/3}$ and $v_l = 1.65v_t$ (see text) where l and t refer to longitudinal and transverse modes. Transverse speeds of sound for the remaining samples were measured in this study (for $x = 0.025$, 0.05, ~ 0.1 , $T = 70$ mK; for $x = 0.76$, $T = 300$ K). A refers to the cross sectional areas of the thermal conductivity samples. The Casimir limit, Λ/T^3 , was calculated from A and the Debye velocities. The Debye lattice contribution to the heat capacity, C_D/T^3 , was calculated from Θ_D for NaCl and was obtained from a fit to the heat-capacity data for NaCN.

Material	ρ (g/cm ³)	Θ_D (K)	v_D (10 ⁵ cm/s)	v_t (10 ⁵ cm/s)	A (cm ²)	Λ/T^3 (W/cm K ⁴)	C_D/T^3 (J/g K ⁴)
NaCl	2.19	321	3.04	2.75	0.3 × 0.3	1.3×10^{-1}	2.02×10^{-6}
$x = 0.025$			3.03	2.19	0.19 × 0.24	9.5×10^{-2}	
$x = 0.05$			3.02	2.09	0.19 × 0.34	1.1×10^{-1}	
$x \sim 0.1$	2.16			1.86	0.31 × 0.31		
$x = 0.76$	1.72			1.50	0.25 × 0.38		
NaCN	1.63	220	2.74	2.48			3.7×10^{-6}

the cross sectional area of the sample and the Debye velocity estimated from the values for NaCl and NaCN (see Table II). For $x = 0.05$ (solid triangles) the thermal conductivity below 1 K is less than the T^3 Casimir prediction (which is $\sim 20\%$ greater than for the $x = 0.025$ sample and is omitted for clarity; see Λ/T^3 in Table II), indicating the presence of an additional scattering mechanism. For $x \sim 0.1$ (open triangles) the thermal conductivity data differ significantly from the lower concentration samples. (Note that $x = 0.2$ is the concentration in the melt and that the CN^- concentration in the solid is estimated to be $x \sim 0.1$; see Sec. III.) Below 1 K the data follow a $T^{2.2}$ power law and approach a magnitude above 40 K which is more similar to a glass than a pure crystal. Although much smaller than in pure NaCl, there is still a peak near the 10 K in the thermal conductivity at this concentration.

Due to the difficulty in growing $(\text{NaCl})_{1-x}(\text{NaCN})_x$ mixed crystals at intermediate CN^- concentrations (see Sec. III), the mixed crystal with the next highest CN^- concentration is $x = 0.76$. [Note that this is in the concentration region ($0.65 \leq x \leq 0.8$) where structural studies show coexistence between the glasslike and ordered phases.⁴⁰] For this concentration (solid circles), the thermal conductivity has both a magnitude and temperature dependence which are very similar to amorphous solids, as shown with the data for $\alpha\text{-SiO}_2$ (dotted curve³⁵). Below 1 K the temperature dependence, $T^{1.9}$, falls within the range typically found for amorphous solids, $T^{2-\delta}$ with $0 \leq \delta \leq 0.2$; the magnitude is a factor of 2 below the range known for amorphous solids.⁴¹ At intermediate temperatures ($5 \text{ K} \leq T \leq 15 \text{ K}$) many amorphous solids exhibit a nearly temperature-independent thermal conductivity referred to as a plateau.⁴² For $x = 0.76$ there is a shoulder near 10 K rather than an identifiable plateau. Since the thermal conductivity below 1 K is quite low, the temperature region over which a plateau would appear seems to have been compressed and only a shoulder

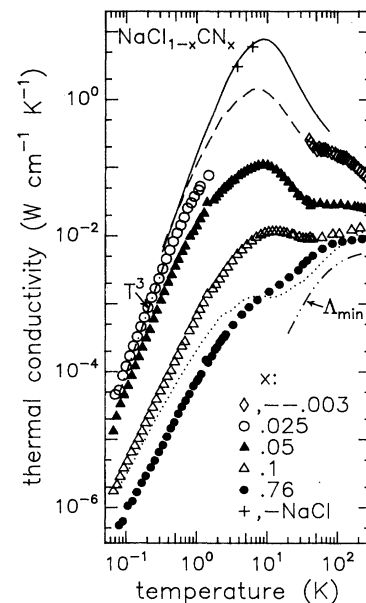


FIG. 4. Thermal conductivity Λ of several concentrations of CN^- in NaCl. Sample dimensions for this work are listed in Table II. All sample surfaces have been roughened with fine grit sandpaper in order to ensure diffuse phonon scattering. NaCl and NaCl+0.3% CN data below 100 K, Ref. 11; measurements between 40 and 300 K on a sample from the same boule have been found to be in excellent agreement in the temperature region of overlap; NaCl, plusses, this work; data for $x = 0.025$, 0.05, ~ 0.10 , 0.76 this work (note that $x = 0.2$ is the value in the melt and that $x \sim 0.1$ is an estimate of the value in the crystal; see Sec. III); data for $\alpha\text{-SiO}_2$, dotted line, Ref. 35. As the CN^- concentration is increased from 0 to 76%, the behavior of Λ below 1 K changes from crystalline (Casimir prediction for $x = 0.025$, dash-dotted line) to glasslike ($x = 0.76$). Dash-dotted curve labeled Λ_{min} is a prediction of the thermal conductivity of 0.76 above 50 K based on the model of Ref. 36 using no adjustable parameters Ref. 37.

remains.

Near room temperature the thermal conductivity of $x=0.76$ is temperature independent, which is another characteristic feature of amorphous solids. At these relatively high temperatures, where the mean-free-path in amorphous solids is on the order of an interatomic spacing⁴³ and the concept of a propagating mode is difficult to justify, it is more appropriate to think of heat transport via a random walk of energy as originally proposed by Einstein⁴⁴ and recently developed by Cahill and Pohl.^{36,45} The same concepts appear to apply to mixed crystals with glasslike excitations.⁹ The dashed-dotted curve labeled Λ_{\min} in Fig. 4 indicates the thermal conductivity based on this model, using no adjustable parameters.³⁷

The data for $x=0.76$ can be used to extract information on the TLS. The tunneling model expression for the thermal conductivity below 1 K due to resonant scattering of phonons from TLS is¹⁴

$$\Lambda(T) = \frac{k_B^3}{6\pi\hbar^2} \left[\sum_{\alpha} \frac{\rho v_{\alpha}}{\bar{P}\gamma_{\alpha}^2} \right] T^2, \quad (1)$$

where ρ is the mass density, v is the sound velocity, \bar{P} is the spectral density of TLS, γ is the coupling energy of TLS to phonons, and α is the transverse or longitudinal mode. In order to extract $\bar{P}\gamma_{\alpha}^2$ we assume the empirical relations $v_l = 1.65v_t$ and $\gamma_l^2 = 2.5\gamma_t^2$, which appear to be good approximations for all amorphous solids.⁴⁶

Although we have not measured the thermal conductivity for pure NaCN, we expect it to be similar to the thermal conductivity of pure KCN (see Fig. 6 of Ref. 4) which is not glasslike. The data of pure KCN show a peak near 10 K, a T^3 temperature dependence below 1 K, and a low magnitude that was ascribed to phonon scattering from domain walls.⁴

B. Specific heat

Long-time ($t \sim 10$ sec) specific-heat data below 1 K for pure NaCl and NaCN, and $(\text{NaCl})_{1-x}(\text{NaCN})_x$ samples with $x=0.05$, ~ 0.1 , and 0.76 are shown in Figs. 5–7. Data obtained by Seward, Reddy, and Shaner for $x=3 \times 10^{-3}$ are shown by the dash-dotted line in Fig. 5.¹⁹ The specific heat of NaCl (asterisks) is Debye-like with a temperature behavior close to T^3 and a magnitude in agreement with the value determined by Lewis, Lehoczky, and Briscoe from the low-temperature elastic constants of NaCl [Figs. 5 and 6, solid line calculated for $\Theta_D = 321$ K (Ref. 38)]. Note also the good agreement with the experimental data by Morrison, Patterson, and Dugdale,⁴⁷ Fig. 6. Approximately 40% of the upturn below 300 mK is estimated to be due to addenda. The most likely residual impurity, OH^- , is expected from thermal conductivity measurements to have a tunnel splitting which would lead to a peak in the specific heat at ~ 0.9 K (Ref. 32) (see also p. 219 of Ref. 12). However, the identity of the scattering center in the NaCl thermal conductivity data in Ref. 32 was not unambiguously determined. If the tunnel splitting were smaller than estimated in Ref. 32 (0.24 cm^{-1} instead of 1.5 cm^{-1}), 0.3 ppm of OH^- with a Schottky peak near 0.1 K

would account for the remaining 60% upturn in our data, in agreement with the uv analysis of our sample.

Increasing the CN^- concentration from $x=3 \times 10^{-3}$ to $x=0.05$ (solid triangles) and $x \sim 0.1$ (open triangles) reduces the magnitude of the specific heat. This indicates that with increasing cyanide concentration, the CN^- have a broader range of tunnel splitting and asymmetry energies and, therefore, do not show up as a single Schottky peak in the specific heat. Their effect is distributed over a large temperature range.

For $x=0.76$, the heat capacity is distinctly different from the low concentration samples. The magnitude and temperature behavior of the specific heat are glasslike, with a temperature dependence $C(T) = c_1 T + (c_D + c_3)T^3$, where $c_D T^3$ is the Debye contribution to the specific heat and c_1 and c_3 are constants (see solid line through data for $x=0.76$ and Fig. 7). In addition, the temperature decays after application of the heat pulses are exponential to within experimental error [Fig. 3(b)], similar to what is seen for amorphous solids on time scales greater than one second. For $x=0.05$ and $x \sim 0.1$,

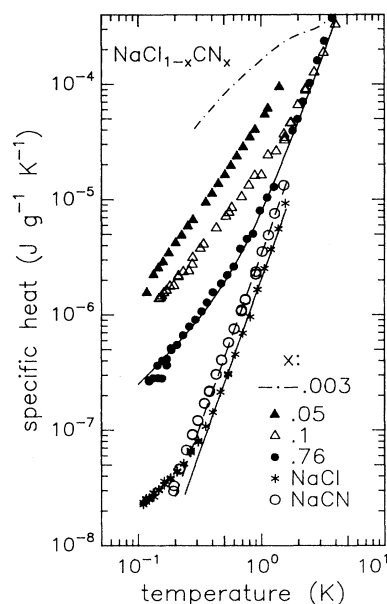


FIG. 5. Long time ($t \sim 10$ sec) specific heat of several $(\text{NaCl})_{1-x}(\text{NaCN})_x$ mixed crystals. Data for $x=0, 0.05, \sim 0.1, 0.76, 1.00$, this work. Dash-dotted line: data for $x=0.003$, Ref. 19. The dashed line through the NaCN data is a T^3 fit from which the Debye temperature and velocity listed in Table II have been determined. The solid line through NaCl is the Debye prediction from Ref. 38 as determined from elastic constant data. For low CN^- concentrations ($x=0.003$) the specific heat is dominated by states of the isolated CN^- [see also Fig. 2(b)]. As the concentration is increased to 76%, the specific heat is dominated by TLS and has a linear term ($c_1 = 2.5 \times 10^{-6} \text{ J g}^{-1} \text{ K}^{-2} = 6.3 \times 10^{-5} \text{ J mol}^{-1} \text{ K}^{-2}$) similar in magnitude to $(\text{KBr})_{0.59}(\text{KCN})_{0.41}$ ($c_1 = 4.4 \times 10^{-5} \text{ J mol}^{-1} \text{ K}^{-2}$ Ref. 4). The solid line through the $x=0.76$ data is a fit of the form $c_1 T + (c_D + c_3)T^3$ (see Fig. 7). The upturn in the data for undoped NaCl below 300 mK is due to residual impurities and addenda which have not been subtracted for this sample.

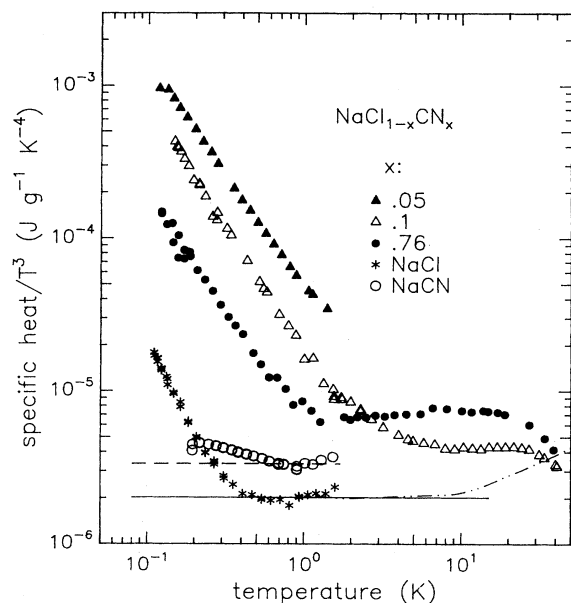


FIG. 6. Specific heat of $(\text{NaCl})_{1-x}(\text{NaCN})_x$, $x = 0.05, \sim 0.1, 0.76$, NaCl, and NaCN plotted as c/T^3 vs T . Dashed and solid straight lines: same as in Fig. 5. Dash-double-dotted line: data for NaCl, Ref. 47.

however, there was evidence of both very short and very long relaxation times, with a clear separation between the two [see Fig. 3(a)]. Upon increasing the CN^- concentration to its maximum value, pure NaCN, the specific heat again varies as T^3 (dashed lines in Figs. 5 and 6), from which we determined the Debye temperature and velocity listed in Table II.

All of these features are similar in $(\text{NaCl})_{1-x}(\text{NaCN})_x$ and $(\text{KBr})_{1-x}(\text{KCN})_x$. In both systems the magnitude of the specific heat below 1 K decreases as the CN^- concen-

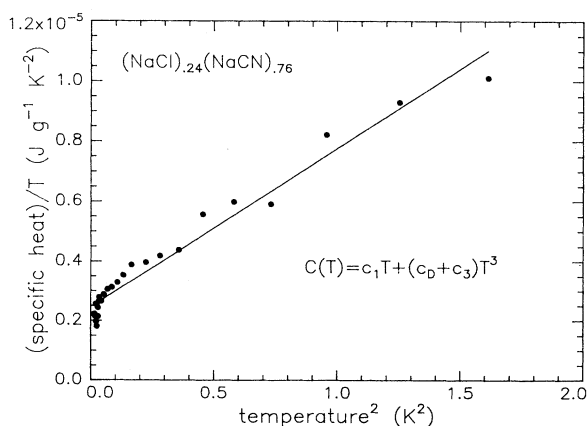


FIG. 7. Specific heat of $(\text{NaCl})_{0.24}(\text{NaCN})_{0.76}$ plotted as C/T vs T^2 to reveal the functional form $C(T) = c_1 T + (c_D + c_3) T^3$. From a linear fit to the data (solid line), $c_1 = 2.5 \times 10^{-6} \text{ J g}^{-1} \text{ K}^{-2}$ and $(c_D + c_3) = 5.3 \times 10^{-6} \text{ J g}^{-1} \text{ K}^{-4}$.

tration is increased from $x \sim 0.05$ to higher concentrations. Also, for $x \leq 0.05$ in $(\text{KBr})_{1-x}(\text{KCN})_x$ there are both very short and long-lived states, but at higher concentrations, in the glasslike range, the temperature decays after application of each heat pulse appear exponential.

The comparison of the specific heat with the thermal conductivity demonstrates a significant difference between the two mixed crystal systems for small CN^- concentrations. Up to $x = 0.025$ in $(\text{NaCl})_{1-x}(\text{NaCN})_x$ the thermal conductivity shows no evidence of resonant scattering of phonons from tunneling states below 1 K (Fig. 4), yet even for $x = 0.003$ the heat capacity is much larger than the Debye lattice contribution (~ 300 times larger at 0.5 K, Fig. 5). In other words, for $x \leq 0.025$ states that show up in the heat capacity do not significantly influence the thermal conductivity below 1 K. By contrast, for similar concentrations of CN^- in KBr the tunneling states produce both a Schottky-type peak in the heat capacity [Fig. 2(a)] and a dip in the thermal conductivity due to resonant scattering (Fig. 1; $T \sim 0.5$ K). This requires some discussion.

Below 1 K, two phonon-scattering mechanisms have to be considered: Scattering from the boundaries of the crystal (Casimir scattering), with a scattering rate $\tau_b^{-1} = v_D l^{-1}$ where v_D is the Debye speed of sound and l is the mean-free-path given by the square root of the cross section of the sample, and resonant scattering of phonons of mode α from the two-level systems, with a scattering rate¹⁴

$$\tau_{\text{res}}^{-1} = \left[\frac{\pi \gamma_\alpha^2 n \omega}{\rho v_\alpha^2} \left(\frac{\Delta_0}{E} \right)^2 \tanh \left(\frac{E}{k_B T} \right) \right] \delta(\hbar\omega - E), \quad (2)$$

where γ_α is the coupling energy of TLS to phonons of mode α , n is the number density of CN^- , ρ is the mass density, v_α is the speed of sound for mode α , and $2E$ is the total energy splitting made up of the tunnel splitting Δ_0 and the asymmetry energy Δ , $2E = (\Delta_0^2 + \Delta^2)^{1/2}$. The thermal conductivity is calculated from a total scattering rate, $\tau^{-1}(T) = \tau_b^{-1} + \tau_{\text{res}}^{-1}(T)$,

$$\Lambda(T) = \frac{1}{3} C v^2 \tau(T), \quad (3)$$

where C is the specific heat of the phonons, and v is an average speed of sound. The resonant scattering rate from TLS must be much less than the boundary scattering rate in order for $\Lambda(T)$ to follow the T^3 Casimir limit below 1 K, as is the case for $x = 0.003$. From Eq. (2) and the expression for τ_b^{-1} , the ratio of the scattering rates in, for example, $x = 0.003$ can be determined, setting conditions on γ , Δ_0 , and E . For simplicity, we assume that the Schottky-like peak near $T_p = 1$ K for $x = 0.003$ [Fig. 2(b)] is due to states with a single energy splitting $E = 2.4 k_B T_p$, where k_B is Boltzmann's constant. Applying the dominant phonon approximation,⁴⁸ these states should cause a resonant dip in the thermal conductivity at a temperature $T_d = E/4.25 k_B = 0.56$ K. Using the Debye velocity and mass density for NaCl in Eq. (2), the number density $n = 6.7 \times 10^{19} \text{ cm}^{-3}$ for $x = 0.003$, and

the cross-sectional area for this sample [$0.5 \times 0.5 \text{ cm}^2$ (Ref. 11)], the ratio of scattering rates at T_p , where τ_{res}^{-1} should be a maximum, is

$$\frac{\tau_{\text{res}}^{-1}}{\tau_b^{-1}} = 4 \times 10^2 \left[\frac{\gamma}{eV} \right]^2 \left[\frac{\Delta_0}{E} \right]^2 \quad (4)$$

(with γ in units of eV). For τ_{res}^{-1} to be less than τ_b^{-1} , either $\gamma < 0.05 \text{ eV}$ or $\Delta_0 < 0.05E$, or some combination of the two. Note that either of these scenarios would also explain the long internal equilibration times observed in the specific heat for small x , since the relaxation time τ_{rel} , the time for an excited state to relax back to its ground state, is given by $\tau_{\text{rel}} \propto \gamma^2 (\Delta_0/E)^2$.¹⁴ We conclude that in order for states to show up in the heat capacity but not in the thermal conductivity in the low CN^- concentration samples, the CN^- must be either weakly coupled to the lattice and/or have very small tunnel splittings Δ_0 .

C. Internal friction and transverse speed of sound

Figures 8 through 13 show the internal friction Q^{-1} and the change in the transverse speed of sound $\delta v/v$ measured in torsion at $\sim 90 \text{ kHz}$ for $(\text{NaCl})_{1-x}(\text{NaCN})_x$,

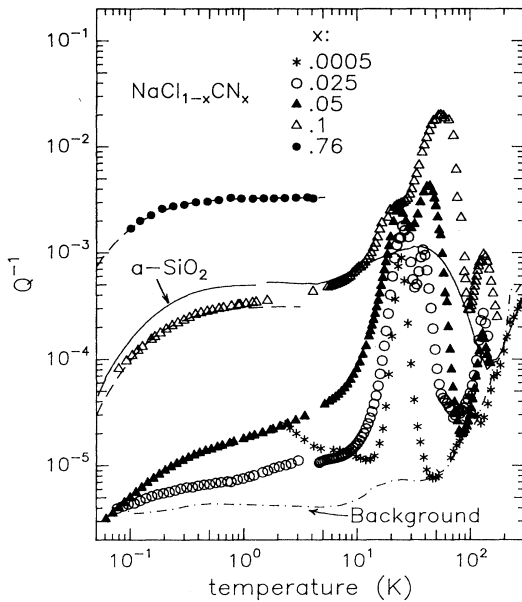


FIG. 8. Internal friction measured in torsion at $\sim 90 \text{ kHz}$ for several $(\text{NaCl})_{1-x}(\text{NaCN})_x$ samples. The dash-dotted curve marked background indicates the loss due to the mounting arrangement and has not been subtracted from the $(\text{NaCl})_{1-x}(\text{NaCN})_x$ data. Solid line: $\alpha\text{-SiO}_2$, Ref. 49 below 1 K and Ref. 45 above 1 K. The two-level-system relaxational contribution to $(\text{NaCl})_{1-x}(\text{NaCN})_x$ below 5 K evolves as the CN^- concentration is increased from 2.5 to 76 %. The dashed lines through data for $x \sim 0.1$ and $x = 0.76$ are fits using the tunneling model prediction. Complicated structure at higher temperatures due to activated processes also develops with increasing CN^- concentration.

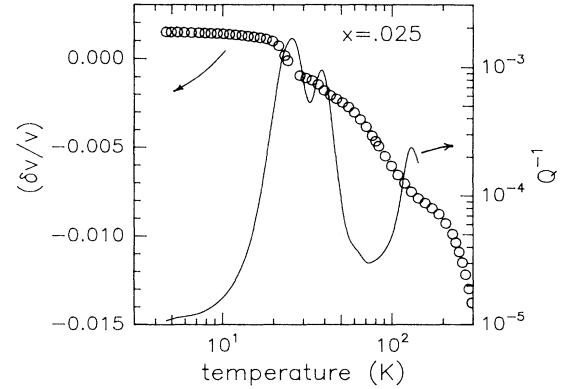


FIG. 9. Variation of the transverse speed of sound for $x = 0.025$ (symbols, left axis). The velocity at 70 mK, $v_t = 2.19 \times 10^5 \text{ cm s}^{-1}$, was chosen as the reference. The material softens monotonically between 4 K and room temperature, with inflection points at temperatures corresponding to the loss peaks (solid line, right axis).

$x = 5 \times 10^{-4}$, 0.025, 0.05, ~ 0.1 , 0.76, and $(\text{KBr})_{0.997}(\text{KCN})_{0.003}$. The curve labeled background in Figs. 8 and 12 indicates the loss due to the mounting arrangement for our crystals (as described in Sec. III C).²⁹ For the lowest concentration measured, $x = 5 \times 10^{-4}$ (asterisks, Fig. 8), a single relaxation peak appears near 25 K. A fit to the peak assuming the form of a Debye relaxation gives a potential barrier for reorientation of 0.03 eV and an attempt frequency of 10^{12} Hz , with a full width at half maximum within 2% of the expected value. The origin of the upturn below 10 K may be an experimental artifact and awaits further study. With increasing CN^- concentration, the magnitude of Q^{-1} increases and three loss peaks appear above 10 K which are presumably due to activation of both individual CN^- and collections of

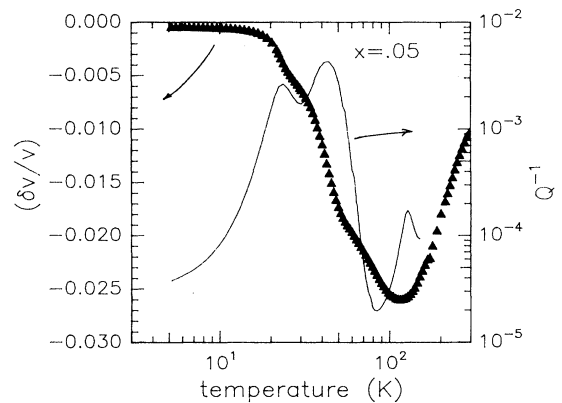


FIG. 10. Variation of the transverse speed of sound for $x = 0.05$. The velocity at 70 mK, $v_t = 2.09 \times 10^5 \text{ cm s}^{-1}$, was chosen as the reference. The material softens between 5 and 100 K and hardens at higher temperatures, see text. Inflection points and minima in $\delta v/v$ are at temperatures corresponding to loss peaks (solid line, right axis).

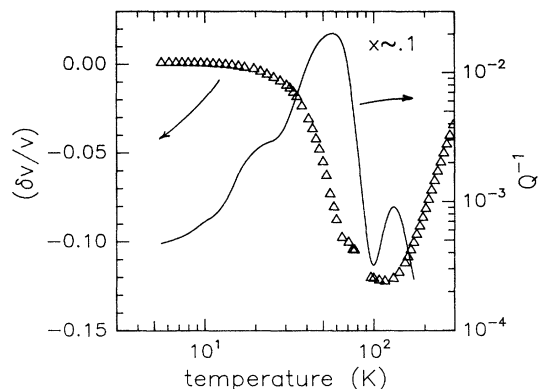


FIG. 11. Variation of the transverse speed of sound for $x \sim 0.1$. The velocity at 70 mK, $v_t = 1.86 \times 10^5 \text{ cm s}^{-1}$, was chosen as the reference. The material softens between 5 and 100 K and hardens at higher temperatures. Inflection points and minima in $\delta v/v$ are at temperatures corresponding to loss peaks (solid line, right axis). No clear evidence of a Bellessa effect can be discerned, probably because of the onset of the structural phase transition. Between 5 and 10 K, $(1/v)(dv/dT) \sim 100 \text{ ppm K}^{-1}$.

CN^- in the lattice.

The peaks in the internal friction above 10 K are reflected in changes in the transverse speed of sound at corresponding temperatures (Figs. 9–11; the speed of sound at $\sim 70 \text{ mK}$ is taken as the reference for computing $\delta v/v$). For $x = 0.025$ (Fig. 9) the speed of sound de-

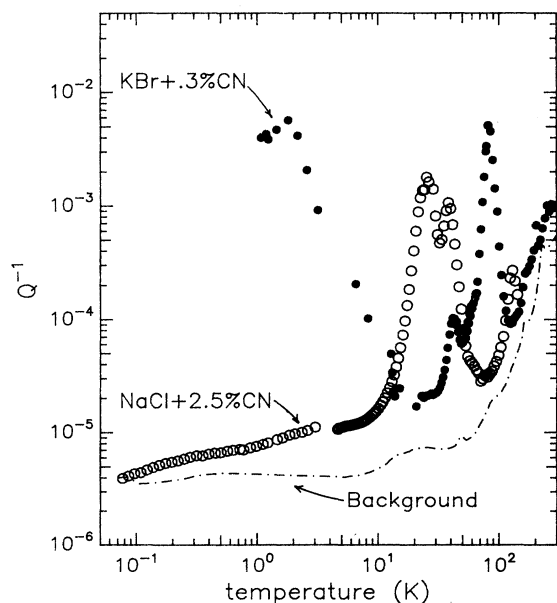


FIG. 12. Comparison of Q^{-1} for $(\text{NaCl})_{1-x}(\text{NaCN})_x$ and $(\text{KBr})_{1-x}(\text{KCN})_x$ at low CN^- concentrations. The significant loss below 5 K for $\text{KBr}+0.3\% \text{CN}$ is absent in the $(\text{NaCl})_{1-x}(\text{NaCN})_x$ sample, supporting the conclusion from the thermal conductivity data: For low CN^- concentrations, CN^- which are mobile in KBr appear to be frozen in NaCl .

creases monotonically with increasing temperature; inflection points appear in $\delta v/v$ at temperatures corresponding to maxima in Q^{-1} . For $x = 0.05$ (Fig. 10) the speed of sound first decreases between 5 and 120 K and then increases again at higher temperatures. This softening at 120 K is a signature of the translational-rotational coupling in the mixed alkali-halide cyanides and has been extensively studied in $(\text{KBr})_{1-x}(\text{KCN})_x$.^{5,6} In pure KCN , for example, the first-order phase transition at 168 K involving alignment of the CN^- elastic quadrupoles is accompanied by nearly complete softening of the transverse-acoustic mode. Dilution of the CN^- by Br^- in $(\text{KBr})_{1-x}(\text{KCN})_x$ reduces the degree of softening and shifts the minimum in $\delta v/v$ to lower temperatures. For $x \sim 0.1$ in $(\text{NaCl})_{1-x}(\text{NaCN})_x$ (Fig. 11) the softening is significant, with a 10% variation in the sound velocity between 120 K and room temperature. For $x = 0.76$ the variation in the sound velocity between 100 K and room

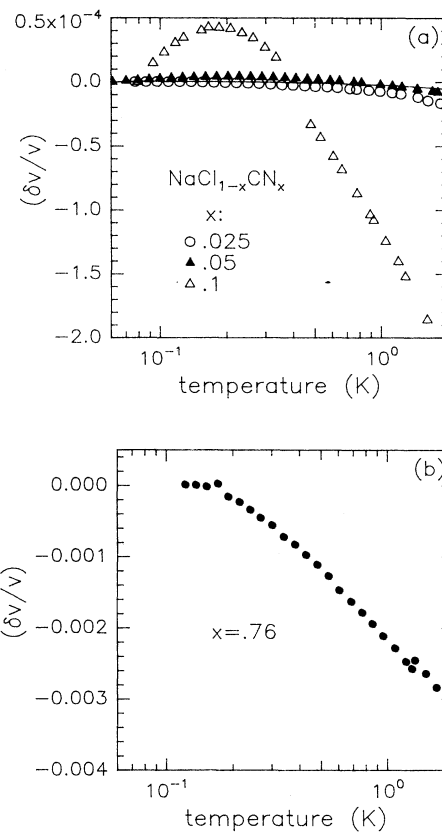


FIG. 13. Variation in the transverse speed of sound below 1 K for $(\text{NaCl})_{1-x}(\text{NaCN})_x$, (a) $x = 0.025, 0.05, \sim 0.1$, and (b) $x = 0.76$; note different vertical scales for (a) and (b). For the lowest concentration samples ($x = 0.025$ and 0.05) the variation is similar to the contribution from the mounting arrangement (solid curve). Only for the higher concentration samples ($x \sim 0.1$ and $x = 0.76$) does the variation become appreciable. Note that the magnitude of $\delta v/v$ for $x = 0.76$ is uncertain by the same factor, $\pm 40\%$, as for the Q^{-1} data for this sample, see text.

temperature was so large that we were unable to track the resonant frequency of our sample. Consequently, Q^{-1} and $\delta v/v$ were only measured below 2 K for this sample.

At temperatures above a few Kelvin, where the internal friction in amorphous solids and mixed crystals with glasslike excitations is dominated by activated processes, the behavior of Q^{-1} is nonuniversal; there is considerable variation between materials in both the magnitude and temperature dependence.⁴⁵ Below 5 K, the temperature dependence of the internal friction has characteristic and universal features due to the relaxation of the low-energy tunneling centers.⁵⁰ Although data for $(\text{NaCl})_{1-x}(\text{NaCN})_x$ are presented over the entire temperature range from 70 mK to 200 K for completeness, we wish to focus the reader's attention on the behavior at low temperatures for a discussion of the evolution of glasslike properties.

Data below 5 K in Fig. 8 illustrate the evolution of glasslike behavior in Q^{-1} for $(\text{NaCl})_{1-x}(\text{NaCN})_x$. For $x=0.025$ (open circles) and $x=0.05$ (solid triangles) the elastic loss below 1 K is small but greater than the background (dash-dotted line). The internal friction data are consistent with the thermal conductivity data for these concentrations; both measurements show little evidence of TLS. A similar concentration of CN^- in KBr, by comparison, gives both strong resonant scattering in the thermal conductivity (Fig. 1) and a large elastic loss (Fig. 12), indicating that the CN^- in KBr are still mobile on the time scale of the inverse probe frequency $[(2\pi\nu)^{-1}=2\times 10^{-6}$ sec]. This is consistent with relaxation times determined for individual tunneling defects in alkali halides, 10^{-5} – 10^{-9} sec (see Table I in Ref. 12). For $x\sim 0.1$ (open triangles, Fig. 8), the internal friction is similar in magnitude to $\alpha\text{-SiO}_2$ (Refs. 45 and 49), although no temperature-independent damping (plateau) is observed. Note that the thermal conductivity, which still shows a small peak around 10 K, also is not exactly glasslike at this CN^- concentration (Fig. 4). For the largest CN^- concentration in our study, $x=0.76$ (solid circles), however, both the elastic loss and the thermal conductivity display the characteristic features of amorphous solids.

The behavior of the relative change in the transverse speed of sound below 1 K is shown in Fig. 13. For the two lowest concentration samples, $x=0.025$ (open circles) and 0.05 (solid triangles) in Fig. 13(a), the variation is similar to what is seen for the mounting arrangement alone (solid curve, see caption). Only for the higher concentration samples, $x\sim 0.1$ [open triangles, Fig. 13(a)] and $x=0.76$ [solid circles, Fig. 13(b)], does the variation become appreciable. Note the different vertical scales in Figs. 13(a) and 13(b).

The temperature dependence of the internal friction in amorphous solids below 5 K can be examined in two limiting cases. In the low-temperature limit, where the probe frequency is large with respect to the maximum relaxation rate of the TLS, $\omega \gg \tau_{\text{max}}^{-1}$, and many states appear to be frozen on the time scale of an oscillation, the internal friction approaches a T^3 temperature dependence (see $\alpha\text{-SiO}_2$ data below 0.1 K, solid line in Fig. 8),^{51,52}

$$Q^{-1} = \frac{\pi^4}{96} \left[\frac{\bar{P}\gamma_t^2}{\rho v_t^2} \right] \left[\frac{T}{T_{\text{co}}} \right]^3, \quad (5)$$

where T_{co} is a characteristic cutoff temperature, defined below. At higher temperatures where the maximum relaxation rate of the TLS is large compared to the probe frequency, $\omega \ll \tau_{\text{max}}^{-1}$, the internal friction is constant (see $\alpha\text{-SiO}_2$ data 1 K $\leq T \leq 5$ K, solid line in Fig. 8),⁵³

$$Q^{-1} = \frac{\pi}{2} \left[\frac{\bar{P}\gamma_t^2}{\rho v_t^2} \right]. \quad (6)$$

The temperature T_{co} , defined by $\omega \coth l = \tau_{\text{max}}^{-1} (E = 2k_B T_{\text{co}})$, indicates the crossover between these two types of behavior. The maximum relaxation rate is given by¹⁴

$$\tau_{\text{max}}^{-1} = \left[\frac{\gamma_l^2}{v_l^5} + 2 \frac{\gamma_t^2}{v_t^5} \right] \frac{E^3}{2\pi\rho\hbar^4} \coth \left[\frac{E}{2k_B T} \right], \quad (7)$$

where the subscripts l and t refer to longitudinal and transverse components. T_{co} is extracted by fitting our data below 1 K to a numerically integrated solution of the TM prediction,¹⁴ the high- and low-temperature limiting expressions of which are given above. (Note that T_{co} is the only parameter used to adjust the fit along the temperature axis.) Given T_{co} , we determine γ_t , the transverse coupling of the TLS to phonons, from the defining relation for T_{co} and the expression for τ_{max}^{-1} .⁵⁴

$$\gamma_t^2 = 1.01 \times 10^{-67} \left[\frac{\rho v_t^5 \nu}{T_{\text{co}}^3} \right], \quad (8)$$

where ρ is the mass density (kg/m^3), v_t is the transverse speed of sound (m/s) determined from the probe frequency and the sample dimensions, ν is the probe frequency (Hz), and γ_t is expressed in Joules. In addition, since the magnitude of Q^{-1} scales as $\bar{P}\gamma_t^2/\rho v_t^2$ according to the tunneling model [see Eqs. (5) and (6)], the fit can be used in conjunction with γ_t to extract \bar{P} .

Tunneling model fits are shown by dashed lines through the data in Fig. 8. Although the thermal and elastic properties of the $x\sim 0.1$ sample are not fully glasslike, the data are fit to the tunneling model for purposes of comparison. Values of \bar{P} and γ_t for $x\sim 0.1$ and $x=0.76$ are listed in Table III along with the values for an amorphous solid, $\alpha\text{-SiO}_2$, a mixed alkali-halide cyanide, $(\text{KBr})_{1-x}(\text{KCN})_x$,⁴ and the system $(\text{NaCN})_{1-x}(\text{KCN})_x$.^{4,56} The transverse coupling of TLS to phonons γ_t is similar in all systems. \bar{P} , the spectral density of states, however, is larger in $(\text{NaCl})_{0.24}(\text{NaCN})_{0.76}$ than in $\alpha\text{-SiO}_2$ or $(\text{KBr})_{0.59}(\text{KCN})_{0.41}$ and is more similar to $(\text{KBr})_{0.81}(\text{KCN})_{0.19}$ and the system $(\text{NaCN})_{1-x}(\text{KCN})_x$. The large error bars for $x=0.76$ reflect the small sample size used for this measurement (see Sec. III). The uncertainty in γ_t for $x=0.76$ is estimated from the combined uncertainties of $\pm 15\%$ for v_t and $\pm 10\%$ for T_{co} .

For a check of the consistency of our analysis, we also extract \bar{P} and γ_t from a tunneling model fit to the $\delta v/v$ data below 1 K. The γ_t values agree with those in Table

TABLE III. Tunneling model parameters γ_i , the transverse coupling energy of TLS to phonons \bar{P} , the spectral density of TLS, and the dimensionless ratio $\bar{P}\gamma_i^2/\rho v_i^2$ [determined from Q^{-1} measurements for the $(\text{NaCl})_{1-x}(\text{NaCN})_x$ samples]. The quantity $\bar{P}\gamma_i^{2*}/\rho v_i^2$ was determined by fitting the thermal conductivity data to T^2 below 1 K and using the values for v_i listed in Table II for $(\text{NaCl})_{1-x}(\text{NaCN})_x$, v_i calculated from elastic constants in Ref. 4 for $(\text{KBr})_{1-x}(\text{KCN})_x$, $v_i = 2.3 \times 10^5 \text{ cm s}^{-1}$ for $(\text{NaCN})_{0.75}(\text{KCN})_{0.25}$ (see Ref. 55), and a transverse speed of sound listed in Ref. 46 for $\alpha\text{-SiO}_2$. For $(\text{KBr})_{1-x}(\text{KCN})_x$, the transverse coupling is determined from the average coupling $\bar{\gamma}$ listed in Ref. 4 using $\gamma_i \sim 0.89\bar{\gamma}$. Note that the $(\text{KBr})_{1-x}(\text{KCN})_x$ CN^- concentrations from Ref. 4 have been updated. Upon additional analysis, $x = 0.50$ in Ref. 4 has been revised to $x = 0.41$, and $x = 0.25$ has been revised to $x = 0.19$; see Ref. 27.

Material	γ_i (eV)	\bar{P} ($10^{44} \text{ J}^{-1} \text{ m}^{-3}$)	$\bar{P}\gamma_i^2/\rho v_i^2 \times 10^4$	$\bar{P}\gamma_i^{2*}/\rho v_i^2 \times 10^4$ ^b	Reference
$(\text{NaCl})_{0.90}(\text{NaCN})_{0.10}$	0.18 ± 0.07	19 ± 6	2.0 ± 0.4^a	2.7 ± 0.6	This work
$(\text{NaCl})_{0.24}(\text{NaCN})_{0.76}$	0.19 ± 0.10	89 ± 42	21 ± 8^a	30 ± 8	This work
$(\text{KBr})_{0.59}(\text{KCN})_{0.41}$	0.16	9 ± 1	2.5^c	1.9	4
$(\text{KBr})_{0.81}(\text{KCN})_{0.19}$	0.11	40 ± 4	4.1^c	3.2	4
$(\text{NaCN})_{0.81}(\text{KCN})_{0.19}$		60 ± 15			56
$(\text{NaCN})_{0.75}(\text{KCN})_{0.25}$				5.3	4
$(\text{NaCN})_{0.41}(\text{KCN})_{0.59}$		45 ± 10			56
$(\text{NaCN})_{0.15}(\text{KCN})_{0.85}$		60 ± 15			56
$\alpha\text{-SiO}_2$	0.65	8	2.8	3.0	35,46

^aFrom internal friction measurements.

^bFrom thermal conductivity measurements.

^cFrom specific-heat measurements.

III to within a few percent. The \bar{P} values determined from the fit to $\delta v/v$ on the high-temperature side of the peak in $\delta v/v$ are $\sim 40\%$ greater than those listed in Table III for $x \sim 0.1$ and $x = 0.76$. Internal friction data compiled in Ref. 49 on Suprasil W measured over a frequency range of 480 Hz–160 kHz suggest that this is not unusual. $\bar{P}\gamma_i^2/\rho v_i^2$ determined from $\delta v/v$ above its peak is typically 40–50% higher than the value determined from Q^{-1} . The reason is unknown, but anharmonic (multiphonon) effects are often suspected.⁵⁷ Finally, we check for agreement between our thermal conductivity and internal friction data by extracting $\rho v_i/\bar{P}\gamma_i^2$ from a T^2 fit to the thermal conductivity below 1 K [see Eq. (1)] and using the transverse sound velocities listed in Table II to obtain the values in column 5 of Table III. $\bar{P}\gamma_i^2/\rho v_i^2$ values from the two experiments agree to within the experimental uncertainties.

V. DISCUSSION

For small CN^- concentrations, $(\text{NaCl})_{1-x}(\text{NaCN})_x$ and $(\text{KBr})_{1-x}(\text{KCN})_x$ behave very differently. At large concentrations, however, both systems are glasslike—not only below x_c (i.e., in the orientational glass state) but also in the concentration region of coexistence of ordered and glasslike structural properties.^{6,27} In the following, we wish to address this remarkable fact. The more firmly one accepts the manner in which TLS evolve in $(\text{KBr})_{1-x}(\text{KCN})_x$, as proposed by Sethna and Chow,⁸ the more extraordinary $(\text{NaCl})_{1-x}(\text{NaCN})_x$ appears. Consider their argument for the origin of the broad distribution of tunneling states in $(\text{KBr})_{1-x}(\text{KCN})_x$, as outlined in cartoon form in Fig. 14. For very low CN^- concentrations [Fig. 14, curve (a)], the potential barrier distribution for 180° reorientations of the CN^- is very narrow and

centered at the small barriers of the isolated CN^- in KBr [essentially the crystal field of KBr, 3 meV (Ref. 11)]. For intermediate CN^- concentrations, Sethna and Chow make the plausible assumption that elastic quadrupole interactions between the CN^- determine the potential barrier distribution and that the crystal field can be ignored. For $x = 0.5$, dielectric measurements⁵⁸ indicate that the peak of the distribution is at 57 meV, a value somewhat less than what one obtains by simply scaling the low-temperature CN^- reorientational barrier in pure KCN [160 meV (Ref. 7)] [57 meV = 71% of $(0.5 \times 160 \text{ meV})$]. In the glasslike concentration range the low potential tail of the distribution peaked at 57 meV [Fig. 14, curve (b), area below dashed line at 8 meV] is associated with the TLS that show up in the specific heat on time scales on the order of 1 sec.^{8,59} Sethna and Chow assume, as in the tunneling model, that there is also a broad distribution of asymmetry energies, and with only one free parameter calculate a time-dependent specific heat that agrees well with the data. Mertz *et al.*⁶⁰ and Ernst *et al.*⁶¹ have extended their arguments to other concentrations of CN^- in KBr with very satisfactory results.

In Fig. 14, curves (c) and (d), analogous cartoons are sketched for $(\text{NaCl})_{1-x}(\text{NaCN})_x$. For low CN^- concentrations, the potential barriers for reorientation are larger than in $(\text{KBr})_{1-x}(\text{KCN})_x$; the peak of the distribution (i.e., the crystal field), therefore, is moved to a higher energy with respect to the same sketch for $(\text{KBr})_{1-x}(\text{KCN})_x$. [A peak at 27 meV is shown in the figure, an average of the values of 17 meV,¹¹ 35 meV,¹³ and 30 meV (this work).] Following the Sethna-Chow argument, at high CN^- concentrations the potential barrier distribution is determined by lattice-mediated elastic quadrupolar interactions between CN^- , and the crystal field can be ignored. If the peak were to scale exactly

with the CN^- concentration it would appear at 76% of the value for pure NaCN [270 meV (Ref. 7)], or at 205 meV. [Since the peak for $(\text{KBr})_{0.5}(\text{KCN})_{0.5}$ is only 71% of the value expected by scaling the barrier for pure

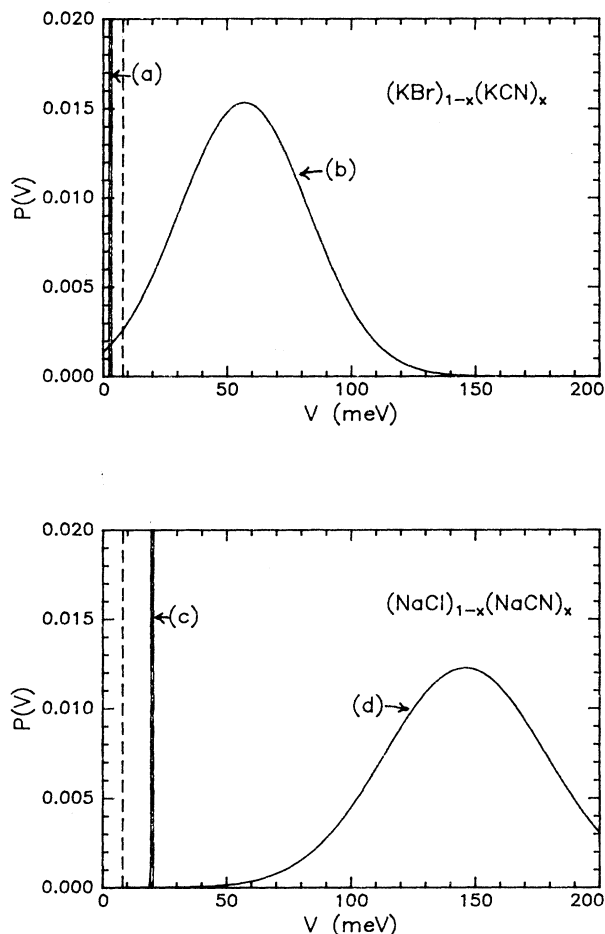


FIG. 14. Cartoon of the potential barrier distribution for 180° rotation of CN^- at $T=0$ K. Curve (a) For small concentrations of CN^- in KBr, the distribution is centered at the relatively small barriers due to the crystal field, 3 meV (Ref. 11). Curve (b) Potential barrier distribution based upon dielectric measurements of $\text{KBr}_{0.5}\text{KCN}_{0.5}$ (Refs. 8 and 58). Lattice mediated interactions between CN^- produce a distribution of barriers with a peak at a much higher energy (~ 57 meV) with respect to curve (a). The states which contribute to the heat capacity on a time scale $t \leq 1$ sec are those with barriers less than 8 meV (dashed line in figure) (Ref. 8). Curve (c) Potential barrier distribution for small concentrations of CN^- in NaCl. The center of the distribution is 6–12 times higher in energy than for KBr+0.3% CN (27 meV is used in the figure). Curve (d) Potential barrier distribution expected for $x=0.76$ neglecting the crystal field and all effects other than lattice-mediated interactions between CN^- . The relative width was chosen to be 25% greater than curve (b). In this oversimplified view, the peak of the distribution is shifted to higher energies with respect to curve (c), leaving an insufficient number of states below 8 meV (dashed line) to account for the thermal and elastic properties below 1 K.

KCN, we conservatively reduce the peak position for $(\text{NaCl})_{0.24}(\text{NaCN})_{0.76}$ by this same factor so that it appears at 146 meV ($=0.71 \times 205$ meV) in Fig. 14 curve (d). Our argument is even stronger if we leave the peak at 205 meV for $x=0.76$. Note also that Elschner *et al.*²⁴ have determined a peak value of 112 meV for $x=0.65$.) The low potential barriers which appear below 8 meV in $(\text{KBr})_{1-x}(\text{KCN})_x$ and are associated with the TLS in that system are missing in $(\text{NaCl})_{1-x}(\text{NaCN})_x$ if the Sethna-Chow argument applies. *There should be no standard glasslike properties in $(\text{NaCl})_{1-x}(\text{NaCN})_x$ if curve (d) is correct.* The fact that glasslike properties *do* appear in $(\text{NaCl})_{1-x}(\text{NaCN})_x$ shows, therefore, that the TLS in $(\text{NaCl})_{1-x}(\text{NaCN})_x$ evolve differently than implied by the Sethna-Chow model for $(\text{KBr})_{1-x}(\text{KCN})_x$.

The specific heat and thermal conductivity data of $(\text{NaCl})_{1-x}(\text{NaCN})_x$ are incompatible with Fig. 14, curve (d). Even for $x \sim 0.10$ the data reveal that there must be states with a tunnel splitting Δ_0 large enough to show up above 100 mK. The thermal conductivity, which is most sensitive to symmetric states, could not be as low as it is below 1 K for $x \sim 0.10$ without the presence of Δ_0 in the range $4.25k_B \times (100 \text{ mK to } 1 \text{ K})$. At some concentration between $x=0.003$, where the thermal conductivity shows no evidence of phonon scattering from TLS, and $x \sim 0.10$, states with low potential barriers (corresponding to larger Δ_0 's) are created, and, with increasing CN^- concentration, have the correct distribution to give glasslike thermal and elastic properties. In other words, tunneling centers which are frozen in the lattice for low concentrations of CN^- appear to become mobile at large x . The system $\text{Ba}_{1-x}\text{La}_x\text{F}_{2-x}$ shows similar behavior.¹⁰ For small x ($x \leq 0.01$) and low temperatures, the tunneling defects are essentially frozen in the lattice. At higher concentrations ($x \geq 0.05$), however, the defects become mobile and have the correct distributions to give the universal low temperature glasslike properties.

We mention two possibilities for the origin of the mobile defects in $(\text{NaCl})_{1-x}(\text{NaCN})_x$ for large x . Sethna has suggested that lattice-mediated elastic quadrupolar interactions between CN^- may reduce the crystal field, creating states with the larger tunnel splittings appropriate for the TLS.⁶² In other words, in addition to curve (d) in Fig. 14, a small fraction of states from curve (c), significantly broadened by elastic quadrupolar interactions, may exist. If this is the case, the low barrier tail extrapolated from dielectric measurements near the peak of the barrier distribution should underestimate the TLS barriers. Dielectric measurements on $(\text{NaCl})_{1-x}(\text{NaCN})_x$ would be interesting to pursue in order to clarify this point.

A second possibility is that random strain fields in $(\text{NaCl})_{1-x}(\text{NaCN})_x$ are responsible for creating the mobile defects by reducing the crystal field associated with a fraction of the CN^- . The system $(\text{NaCN})_{1-x}(\text{KCN})_x$ is also interesting in regard to the creation of states with low potential barriers. Single crystal NaCN and KCN do not individually exhibit low-temperature glasslike properties.⁶³ Lattice-mediated in-

teractions between the CN^- in these pure alkali cyanides create large reorientational barriers for the CN^- [0.16 eV for KCN and 0.27 eV for NaCN (Ref. 7)]. Yet, upon mixing the two materials, the high-temperature orientational phase transitions are suppressed and glasslike excitations appear at low temperatures.^{4,56,64,65} By introducing random strains through the substitution of K for Na, states with significantly lower energies than for pure NaCN or KCN are created for intermediate concentrations. Recent experimental work on the compounds $(\text{KBr})_{1-x}(\text{KCl})_x + 1\% \text{CN}$ (Ref. 66) and Kr^{14}N_2 (Ref. 67) and theoretical work on $(\text{KBr})_{1-x}(\text{KCN})_x$ (Ref. 68) demonstrate more directly that static random strains are capable of creating broad energy distributions for tunneling centers in mixed crystals with glasslike properties. Similarly, random strains may lead to the glasslike excitations observed in many disordered crystalline systems, as in $\text{Ba}_{1-x}\text{La}_x\text{F}_{2-x}$.^{9,10}

VI. SUMMARY

Thermal conductivity, specific heat, and internal friction data indicate that $(\text{NaCl})_{0.24}(\text{NaCN})_{0.76}$ has glasslike properties. The manner in which the TLS evolve, howev-

er, is strikingly different from the model of Sethna and Chow where elastic quadrupolar interactions between the CN^- are directly responsible for the potential barrier distribution of the low-energy excitations in $(\text{KBr})_{1-x}(\text{KCN})_x$. By contrast, for $(\text{NaCl})_{1-x}(\text{NaCN})_x$, the most likely causes for the glasslike low-energy states of the CN^- tunneling centers are the effects of random strains and elastic quadrupolar interactions on the crystal field. These findings suggest that similar causes may lead to the glasslike excitations in a wide class of disordered crystals, and conceivably also in amorphous solids.

ACKNOWLEDGMENTS

Conversations with D. G. Cahill, J. P. Sethna, M. Meissner, K. Knorr, and A. Raychaudhuri are gratefully acknowledged. We would like to thank Karen A. Topp and Phat Vu for help with some of the measurements, and Gerhard Schmidt of the MSC Crystal Growing Facility at Cornell for growth of the $(\text{NaCl})_{1-x}(\text{NaCN})_x$ mixed crystals. This work was supported by NSF Grant No. DMR-91-15981. One of the authors (S.K.W.) would like to acknowledge the financial support of TRW Corporation and U. C. San Diego.

*Present address: U.C. San Diego, La Jolla, CA 92093.

¹W. A. Phillips, *J. Low. Temp. Phys.* **7**, 351 (1972).

²P. W. Anderson, B. I. Halperin, and C. M. Varma, *Philos. Mag.* **25**, 1 (1972).

³See the following references for more comprehensive reviews of systems with glasslike properties: A. C. Anderson, *Phase Transitions* **5**, 301 (1985); A. M. de Goër, in *Photon Scattering in Condensed Matter V*, edited by A. C. Anderson and J. P. Wolfe (Springer-Verlag, Berlin, 1986), p. 6; R. O. Pohl, J. J. De Yoreo, M. Meissner, and W. Knaak, in *Physics of Disordered Materials*, edited by David Adler, Hellmut Fritzsche, and Stanford R. Ovshinsky (Plenum, New York, 1985), p. 529; D. G. Cahill, J. R. Olson, Henry E. Fischer, S. K. Watson, R. B. Stephens, R. H. Tait, T. Ashworth, and R. O. Pohl, *Phys. Rev. B* **44**, 12 226 (1991).

⁴J. J. De Yoreo, W. Knaak, M. Meissner, and R. O. Pohl, *Phys. Rev. B* **34**, 8828 (1986). Note that the CN^- values listed in this work have since been slightly revised as shown in Table III (see also Ref. 27).

⁵K. H. Michel, *Phys. Rev. Lett.* **57**, 2188 (1986); *Phys. Rev. B* **35**, 1405 (1987).

⁶K. Knorr, *Physica Scr.* **T19**, 531 (1987).

⁷F. Lüty, in *Defects in Insulating Crystals*, edited by V. M. Turkevich and K. K. Swartz (Springer-Verlag, Berlin, 1982), p. 69.

⁸James P. Sethna and Kenneth S. Chow, *Phase Transitions* **5**, 317 (1985); M. Meissner, W. Knaak, James P. Sethna, Kenneth S. Chow, J. J. DeYoreo, and R. O. Pohl, *Phys. Rev. B* **32**, 6091 (1985).

⁹David G. Cahill, S. K. Watson, and R. O. Pohl, *Phys. Rev. B* **46**, 6131 (1992).

¹⁰David G. Cahill and R. O. Pohl, *Phys. Rev. B* **39**, 10477 (1989).

¹¹W. D. Seward and V. Narayanamurti, *Phys. Rev.* **148**, 463 (1966).

¹²V. Narayanamurti and R. O. Pohl, *Rev. Mod. Phys.* **42**, 201

(1970).

¹³N. E. Byer and H. S. Sack, *Phys. Status Solidi* **30**, 569 (1968).

¹⁴W. A. Phillips, *Rep. Prog. Phys.* **50**, 1657 (1987). Equation (3.3) shows that the photon-scattering rate scales directly with the TLS energy splitting. Equation (2.26) gives the expression for the relaxation rate of the TLS. Equation (4.34) gives the relaxational contribution to the acoustic loss.

¹⁵F. C. Baumann and R. O. Pohl, *Phys. Rev.* **163**, 843 (1967).

¹⁶P. P. Peressini, Ph. D. thesis, Cornell University, Ithaca, 1983.

¹⁷J. N. Dobbs, M. C. Foote, and A. C. Anderson, *Phys. Rev. B* **33**, 4178 (1986).

¹⁸Note, however, that M. Klein has argued that glasslike properties are even apparent at concentrations as small as 300 ppm CN^- , Michael W. Klein, *Phys. Rev. Lett.* **65**, 3017 (1990); in response to that argument, see the comment by R. O. Pohl and M. Meissner, *Phys. Rev. Lett.* **67**, 1469 (1991), and Klein's response.

¹⁹W. D. Seward, V. Reddy, and J. W. Shaner, *Solid State Commun.* **11**, 1569 (1972).

²⁰S. Haussühl, J. Eckstein, K. Recker, and F. Wallrafen, *Acta Crystallogr. A* **33**, 847 (1977).

²¹*CRC Handbook of Chemistry and Physics*, 67th ed., edited by Robert C. Weast (CRC Press, Boca Raton, 1986), p. E-207.

²²T. Schröder, A. Loidl, and T. Vogt, *Phys. Rev. B* **39**, 6186 (1989).

²³Michael W. Klein, Baruch Fischer, A. C. Anderson, and P. J. Anthony, *Phys. Rev. B* **18**, 5887 (1978).

²⁴S. Elschner, J. Albers, A. Loidl, and J. K. Kjems, *Europhys. Lett.* **4**, 1139 (1987).

²⁵E. T. Swartz, *Rev. Sci. Instrum.* **57**, 2848 (1986).

²⁶David G. Cahill, *Rev. Sci. Instrum.* **61**, 802 (1990).

²⁷Susan K. Watson, David G. Cahill, and R. O. Pohl, *Phys. Rev. B* **40**, 6381 (1989).

²⁸D. G. Cahill and J. E. Van Cleve, *Rev. Sci. Instrum.* **60**, 2706 (1989).

²⁹Note that for $(\text{NaCl})_{1-x}(\text{NaCN})_x$ samples with less than 10%

- CN⁻, including the background has the effect of making the internal friction data fall off more slowly below ~200 mK. For the higher concentration samples, the background makes only a small contribution to the data below ~50 K and can be neglected.
- ³⁰A. K. Raychaudhuri and R. O. Pohl, *Phys. Rev. B* **46**, 10 657 (1992).
- ³¹Miles V. Klein, S. O. Kennedy, Tan Ik Gie, and Brent Wedding, *Mater. Res. Bull.* **3**, 677 (1968).
- ³²Ralph L. Rosenbaum, Cheuk-Kin Chau, and Miles V. Klein, *Phys. Rev.* **186**, 852 (1969).
- ³³Two NCO⁻ peaks at ~630 and ~1205 cm⁻¹ were used to determine the NCO⁻ impurity concentrations. (The fundamental vibration for NCO⁻ is obscured by the CN⁻ absorption peak.) The values of σ for the two peaks were estimated from the value for the NCO⁻ fundamental ($\sigma = 7 \times 10^{17}$ cm⁻²) at 2182 cm⁻¹ in KCl measured by R. Pompei, see Ref. 11, p. 465. An IR scan was performed on a crystal from the same boule as Pompei used and, by comparing the magnitudes of the peaks at 630, 1205, and 2182 cm⁻¹, we estimated values of $\sigma = 8.6 \times 10^{18}$ cm⁻² for the peak at 630 cm⁻¹ and $\sigma = 1.2 \times 10^{19}$ cm⁻² for the peak at 1205 cm⁻¹.
- ³⁴J. K. Krüger, R. Jimenez, K.-P. Bohn, J. Petersson, J. Albers, A. Klöpperpieper, E. Sauerland, and H. E. Müser, *Phys. Rev. B* **42**, 8537 (1990).
- ³⁵See α -SiO₂ data by Raychaudhuri *et al.* in the following: David G. Cahill and R. O. Pohl, *Ann. Rev. Phys. Chem.* **39**, 93 (1988).
- ³⁶D. G. Cahill and R. O. Pohl, *Solid State Commun.* **70**, 927 (1989).
- ³⁷The input to the theory includes the number of atoms (Na, Cl, CN) per unit volume ($n = 4.04 \times 10^{22}$ cm⁻³) calculated from the lattice constant ($a = 5.828$ Å) measured at 290 K by x-ray diffraction; and the transverse ($v_t = 1.5 \times 10^5$ cm s⁻¹) and longitudinal ($v_l = 2.5 \times 10^5$ cm s⁻¹) speeds of sound using $v_l = 1.65v_t$.
- ³⁸J. J. Lewis, A. Lehoczky, and C. V. Briscoe, *Phys. Rev.* **161**, 877 (1967).
- ³⁹Å. V. Karlsson, *Phys. Rev. B* **2**, 3332 (1976).
- ⁴⁰S. Elschner, K. Knorr, and A. Loidl, *Z. Phys. B* **61**, 209 (1985).
- ⁴¹R. O. Pohl, *Phase Transitions* **5**, 239 (1985).
- ⁴²For a discussion of the thermal conductivity plateau, see Mohit Randeria and James P. Sethna, *Phys. Rev. B* **38**, 12 607 (1988) and Eric R. Grannan, Mohit Randeria, and James P. Sethna, *Phys. Rev. B* **41**, 7799 (1990).
- ⁴³R. C. Zeller and R. O. Pohl, *Phys. Rev. B* **4**, 2029 (1971).
- ⁴⁴A. Einstein, *Ann. Phys.* **22**, 180 (1907).
- ⁴⁵David G. Cahill, Ph. D. thesis, Cornell University, Ithaca, 1989.
- ⁴⁶J. F. Berret and M. Meissner, *Z. Phys. B* **70**, 65 (1988).
- ⁴⁷J. A. Morrison, D. Patterson, and J. S. Dugdale, *Can. J. Chem.* **33**, 375 (1955).
- ⁴⁸Tom Klitsner and R. O. Pohl, *Phys. Rev. B* **36**, 6551 (1987).
- ⁴⁹Jeffrey E. Van Cleve, Ph. D. thesis, Cornell University, Ithaca, 1991.
- ⁵⁰Note that the resonant absorption makes an insignificant contribution to Q^{-1} compared to the relaxational absorption at the relatively low excitation frequencies used for our experiments.
- ⁵¹J. E. Van Cleve, A. K. Raychaudhuri, and R. O. Pohl, *Z. Phys. B* **93**, 479 (1994).
- ⁵²S. Hunklinger and W. Arnold, *Physical Acoustics 12*, edited by W. P. Mason and R. N. Thurston (Academic, New York, 1973), p. 155.
- ⁵³J. Jäckle, *Z. Phys.* **257**, 212 (1972).
- ⁵⁴Again, we use the empirical relations $v_t = 1.65v_l$ and $\gamma_t^2 = 2.5\gamma_l^2$, which hold for amorphous solids (Ref. 46).
- ⁵⁵The transverse speed of sound for (NaCN)_{0.75}(KCN)_{0.25} was estimated from the Debye temperature ($\Theta_D \sim 193$ K, Ref. 56) and approximate lattice constant ($a \sim 6.1$ Å) determined from an interpolation between the low-temperature values for NaCN and KCN listed in Ref. 64. In order to relate the transverse speed of sound to the Debye velocity, we used the approximations $v_D^{-3} = 1/3(2v_t^{-3} + v_l^{-3})$ and $v_t = 1.65v_l$ (discussed in text).
- ⁵⁶B. Mertz, J. F. Berret, R. Böhmer, A. Loidl, M. Meissner, and W. Knaak, *Phys. Rev. B* **42**, 7596 (1990).
- ⁵⁷S. Hunklinger and A. K. Raychaudhuri, *Prog. Low Temp. Phys.* **9**, 265 (1986).
- ⁵⁸N. O. Birge, Y. H. Jeong, S. R. Nagel, S. Bhattacharya, and S. Susman, *Phys. Rev. B* **30**, 2306 (1984).
- ⁵⁹Note that the potential barriers responsible for the TLS are not directly measured in the dielectric measurements of Ref. 58. The dielectric loss probes values near the peak of the potential barrier distribution; the barriers important for the TLS are determined from an extrapolation of the distribution to low barrier values.
- ⁶⁰B. Mertz, R. Böhmer, B. Eisele, and A. Loidl, *Z. Phys. B* **79**, 431 (1990).
- ⁶¹Richard M. Ernst, Lei Wu, Sidney R. Nagel, and Sherman Susman, *Phys. Rev. B* **37**, 10 444 (1988).
- ⁶²J. P. Sethna (private communication).
- ⁶³Note, however, that K. Knorr has shown that upon repeated thermal cycling, the phase transitions even in pure KCN can be suppressed. See K. Knorr, *Phys. Rev. Lett.* **66**, 3016 (1991).
- ⁶⁴A. Loidl, T. Schröder, R. Böhmer, K. Knorr, J. K. Kjems, and R. Born, *Phys. Rev. B* **34**, 1238 (1986).
- ⁶⁵Ailan Cheng, Michael L. Klein, and Laurent J. Lewis, *Phys. Rev. Lett.* **66**, 624 (1991).
- ⁶⁶Susan K. Watson, David G. Cahill, and R. O. Pohl (unpublished).
- ⁶⁷M. G. Bagatskii, V. G. Manzhelii, P. I. Muromtsev, and I. Ya. Minchina, *Sov. J. Low Temp. Phys.* **18**, 23 (1992); **18**, 801 (1992).
- ⁶⁸Michael P. Solf and Michael W. Klein, *Phys. Rev. B* **49**, 12 703 (1994).